

Quantum gyroelectric effect: Photon spin-1 quantization in continuum topological bosonic phases

Todd Van Mechelen and Zubin Jacob*

Birck Nanotechnology Center and Purdue Quantum Center, Department of Electrical and Computer Engineering, Purdue University, West Lafayette, Indiana 47907, USA

(Received 8 June 2018; published 21 August 2018)

Topological phases of matter arise in distinct fermionic and bosonic flavors. The fundamental differences between them are encapsulated in their rotational symmetries—the spin. Although spin quantization is routinely encountered in fermionic topological edge states, analogous quantization for bosons has proven elusive. To this end, we develop the complete electromagnetic continuum theory characterizing 2+1D topological bosons, taking into account their intrinsic spin and orbital angular momentum degrees of freedom. We demonstrate that spatiotemporal dispersion (momentum and frequency dependence of linear response) captures the matter-mediated interactions between bosons and is a necessary ingredient for topological phases. We prove that the bulk topology of these 2+1D phases is manifested in transverse spin-1 quantization of the photon. From this insight, we predict two unique bosonic phases—one with even parity $C = \pm 2$ and one with odd $C = \pm 1$. To understand the even parity phase $C = \pm 2$, we introduce an exactly solvable model utilizing nonlocal optical Hall conductivity and reveal a single gapless photon at the edge. This unidirectional photon is spin-1 helically quantized, immune to backscattering, defects, and exists at the boundary of the $C = \pm 2$ bosonic phase and any interface—even vacuum. The contrasting phenomena of transverse quantization in the bulk, but longitudinal (helical) quantization on the edge is addressed as the quantum gyroelectric effect. We also validate our bosonic Maxwell theory by direct comparison with the supersymmetric Dirac theory of fermions. To accelerate the discovery of such bosonic phases, we suggest two probes of topological matter with broken time-reversal symmetry: momentum-resolved electron energy-loss spectroscopy and cold atom near-field measurement of nonlocal optical Hall conductivity.

DOI: [10.1103/PhysRevA.98.023842](https://doi.org/10.1103/PhysRevA.98.023842)**I. INTRODUCTION**

Initial observations of topological phases of matter surfaced with the quantum Hall effect (QHE), a discovery which revealed that the transverse conductivity $\sigma_H = n \frac{e^2}{h}$ is naturally quantized [1–3]. e is the elementary charge of the electron and h is the Planck constant. Here, $n \in \mathbb{Z}$ is the electronic Chern number and represents a global topological invariant. Being a global property of the bulk electronic band structure, it is insensitive to disorder within the material. Yet, in terms of the photon with frequency ω and momentum k ,

$$\sigma_H(0, 0) = n \frac{e^2}{h}, \quad (1)$$

it only describes the local static response $\omega = k = 0$ and contains no information of the high-frequency $\omega > 0$, short-wavelength $k > 0$ behavior of the electromagnetic field. The ac dynamical equivalent $\sigma_H(\omega, 0)$ of the conventional dc conductivity $\sigma_H(0, 0)$ is known as the optical Hall conductivity. It is measured using the Faraday rotation angle (gyrotropic response) and has shown plateaulike behavior up to THz frequencies [4]. The purpose of this paper is to unravel the global topological properties of the photon and the role of spin-1 quantization in the generalized optical Hall conductivity $\sigma_H(\omega, k)$.

Conventionally, topological materials have focused on fermionic behavior, which display spin-1/2 polarized edge states and integer quantization of the Hall conductivity [5,6]. However, spin-1 bosonic phases with broken time-reversal symmetry (TRS) have recently been proposed [7–14] and correspond to *even* integer Hall quantization. Pioneering research in topological photonics has mimicked the fermionic behavior using carefully structured pseudo-spin-1/2 photonic crystals [15–19]. A few striking examples are gyrotropic photonic crystals [20–22], Floquet topological insulators [23], and bianisotropic metamaterials [24–26] which support chiral photonic edge states. Similar pseudospin approaches utilizing Haldane models on honeycomb lattices have led to Chern insulators [27]. These are quantum Hall phases but with zero field—realized in photonic crystals, circuit QED [28], and cold atom systems [29]. Important work has also developed Chern invariants for continuous photonic media with broken TRS [30–33]. Nevertheless, the discovery of true spin-1 quantized phases has remained an open problem, as well as the connection between bosonic and photonic topologies. We solve both these problems simultaneously which can open interesting avenues for condensed-matter physics and photonics.

The essential difference between fermions and bosons is revealed in their half-integer vs integer spins. This difference is directly reflected in single-particle geometric phases [34,35] and arises from their rotational symmetries (\mathcal{R}). Under cyclic revolution, a fermion returns out of phase with itself $\mathcal{R}(2\pi) = -1$, meaning topological monopoles exhibit half-integer quantization. Conversely, bosons return in phase under

*zjacob@purdue.edu

the same rotation $\mathcal{R}(2\pi) = +1$, signaling integer monopoles in the band structure. Due to this critical distinction, fermions and bosons constitute different topological classes which are incommensurable with one another. Although a host of naturally occurring fermionic phases have been discovered [36], no bosonic equivalent has been found to date. In this paper, we develop the theory of TRS broken bosonic phases for light to accelerate their discovery.

We put forth the complete microscopic continuum theory describing all 2+1D bosonic phases of the photon. We account for the inherent spin-1 symmetries of the electromagnetic field such that the bosonic properties emerge naturally. This marks a distinct departure from previous attempts at building topological field theories for the photon. We reveal that the signature of these topological bosonic phases is bulk transverse spin quantization [37–40]—in stark contrast to conventional photonic media where transverse spin is a continuous classical number. From very general symmetry arguments, we predict two unique photonic phases, with even $C = \pm 2$ or odd $C = \pm 1$ parity.

We show the fundamental necessity of spatiotemporal dispersion (momentum and frequency dependence of linear response) to define global topological invariants in continuum phases of matter. Spatiotemporal dispersion is a natural consequence of matter-mediated interactions between bosonic fields. We introduce an exactly solvable model, exploiting nonlocal optical Hall conductivity $\sigma_H(\omega, k)$, to unravel the topological physics of the even parity phase $C = \pm 2$. This phase has been predicted in interacting bosonic systems and corresponds to a single gapless photon at the edge. The unidirectional photon exists at the boundary of the nontrivial gyrotropic medium and arbitrary material interface, unlike any previously known edge states in electromagnetism. It hosts many intriguing optical properties, such as spin-1 helical quantization, anomalous displacement currents, and robustness to disorder. We address the contrasting phenomena of transverse quantization in the bulk and longitudinal (helical) quantization at the edge as the quantum gyroelectric effect (QGEE). To rigorously validate our bosonic predictions, we directly compare this model to its supersymmetric Dirac theory [41–44], highlighting the striking similarities, but important differences, between spin-1 and spin-1/2 topologies. Finally, we suggest experimental probes to search for these bosonic phases of matter.

This article is organized as follows. In Sec. II we analyze the linear response theory of 2+1D electromagnetism and derive the regularized continuum Hamiltonian with broken TRS. In Sec. III we study the rotational symmetries of this Hamiltonian and discuss the physical implications of orbital, spin, and total angular momentum of the collective light-matter excitations. The following Sec. IV relates integer spin directly to the Chern number and all topological bosonic phases of the photon are found. Using an exactly solvable model, the even parity bosonic phase $C = \pm 2$ is examined extensively. Section V validates our predictions by directly comparing the Maxwell model to its supersymmetric Dirac theory. This procedure highlights the correspondence between traditional fermionic phases and even parity bosonic phases, while also elucidating the fundamental role of spin. Section VI presents our conclusions and a discussion of how to search for bosonic phases in gyrotropic plasmas and quantum wells. We anticipate

the development of new experimental tools to probe the signatures of these spin-1 quantized photonic edge states.

The focus of this paper is TRS broken topological bosonic phases which possess unidirectional edge states. As mentioned above, this is fundamentally related to optical Hall conductivity and gyrotropy in matter. However, TRS protected bosonic phases are also possible and show counterpropagating edge states [14]. This arises from antisymmetric magnetoelectricity as opposed to gyrotropy. The hallmark of both these bosonic phases is longitudinal spin-1 quantization at the edge. These topologically protected edge states are emergent massless photons with massivelike photons in the bulk material. The rigorous validity of these topological bosonic phases follows from supersymmetric Dirac theory and constitutes a one-to-one mapping to the continuum fermionic phase. This direct analogy between Dirac-fermions and Maxwell-bosons (see Fig. 1) fundamentally requires spatiotemporal dispersion.

II. CONTINUUM TOPOLOGICAL PHOTONICS

A. 2+1D electrodynamics

In two spatial dimensions (and one temporal dimension), the propagation of charge is restricted to the x - y plane. This limits the degrees of freedom of both the electromagnetic field and the induced response of a material (Fig. 2). Therefore, we focus on strictly transverse-magnetic (TM) waves, meaning there are only three unique components of the field. From first principles (Appendix A 1), we derive the corresponding wave equation of the 2D photon coupled to matter,

$$\mathcal{H}_0(\mathbf{k})f = \omega\mathcal{M}(\omega, \mathbf{k})f, \quad f = \begin{bmatrix} E_x \\ E_y \\ H_z \end{bmatrix}, \quad (2)$$

where f is the TM polarization state (wave function) of the electromagnetic field. In the absence of matter, $\mathcal{H}_0(\mathbf{k})$ are the vacuum Maxwell equations in momentum space,

$$\mathcal{H}_0(\mathbf{k}) = k_x \hat{S}_x + k_y \hat{S}_y = \begin{bmatrix} 0 & 0 & -k_y \\ 0 & 0 & k_x \\ -k_y & k_x & 0 \end{bmatrix}. \quad (3)$$

Notice that $\mathcal{H}_0(\mathbf{k}) = \mathbf{k} \cdot \mathbf{S}$ represents optical helicity, i.e., the projection of momentum \mathbf{k} onto the spin \mathbf{S} . We identify these spin-1 operators \hat{S}_x and \hat{S}_y that satisfy the angular momentum algebra $[\hat{S}_x, \hat{S}_y] = i\hat{S}_z$,

$$\hat{S}_x = \begin{bmatrix} 0 & 0 & 0 \\ 0 & 0 & 1 \\ 0 & 1 & 0 \end{bmatrix}, \quad \hat{S}_y = \begin{bmatrix} 0 & 0 & -1 \\ 0 & 0 & 0 \\ -1 & 0 & 0 \end{bmatrix},$$

$$\hat{S}_z = \begin{bmatrix} 0 & -i & 0 \\ i & 0 & 0 \\ 0 & 0 & 0 \end{bmatrix}. \quad (4)$$

Here, $(\hat{S}_z)_{ij} = -i\epsilon_{ijz}$ is the generator of rotations in the x - y plane and is represented by the antisymmetric matrix. \hat{S}_z will be foundational when discussing spin-1 symmetries in two dimensions.

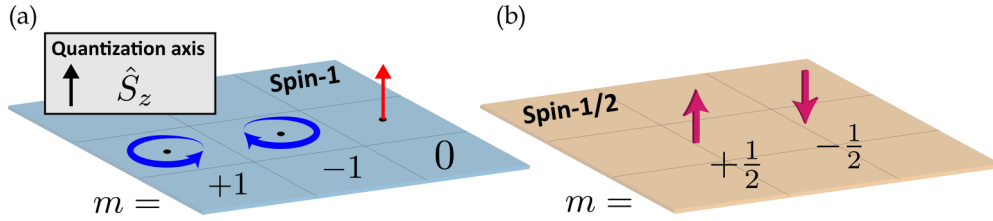


FIG. 1. Our work emphasizes the fundamental differences between 2+1D topological materials for Maxwell bosons and Dirac fermions, which are characterized by their bulk spin quantum numbers. In two dimensions, the quantization axis is along z as all rotations occur in the x - y plane. Both (a) photonic and (b) electronic topologies are connected to \hat{S}_z quantization at certain high-symmetry \mathbf{k} points in the bulk material. The distinction lies in their rotational symmetries (\mathcal{R}). Photons are bosonic particles and respect spin-1 statistics $\mathcal{R}(2\pi) = +1$, which possess integer spin projections $m = \pm 1, 0$. Conversely, electrons are fermionic particles and respect spin-1/2 statistics $\mathcal{R}(2\pi) = -1$, which possess half-integer spin projections $m = \pm \frac{1}{2}$. This changes the interpretation of topological invariants and the observable phenomena of different particles.

The linear response function of the 2D material \mathcal{M} is dependent on continuous variables ω and \mathbf{k} ,

$$\mathcal{M}(\omega, \mathbf{k}) = \begin{bmatrix} \epsilon_{xx} & \epsilon_{xy} & \chi_x \\ \epsilon_{xy}^* & \epsilon_{yy} & \chi_y \\ \chi_x^* & \chi_y^* & \mu \end{bmatrix}, \quad \begin{aligned} D_i &= \epsilon_{ij} E^j + \chi_i H_z, \\ B_z &= \chi_i^* E^i + \mu H_z, \end{aligned} \quad (5)$$

which compactly represents the constitutive relations. We include all possible material responses as a generalization—for instance magnetoelectricity χ_i and birefringence in ϵ_{ij} . However, based on symmetry constraints, we will show that only certain parameters of \mathcal{M} are important in the topological classification.

B. Continuum response function

Alas, Eq. (2) poses a problem; it does not represent a proper first-order in time Hamiltonian since the response function $\mathcal{M}(\omega, \mathbf{k})$ is dependent on its own eigenvalue. Nevertheless, we can prove that it is derived from a first-order Hamiltonian by exploiting stringent symmetry properties. We demand Hermiticity $\mathcal{M} = \mathcal{M}^\dagger$ such that the response is lossless. We also require positive definiteness $\bar{\mathcal{M}} = \partial_\omega(\omega\mathcal{M}) > 0$ to ensure the energy density is non-negative and admits proper normalization $f^\dagger \bar{\mathcal{M}} f > 0$. The response must be causal (Kramers-Kronig) and obey the reality condition $\mathcal{M}(\omega, \mathbf{k}) = \mathcal{M}^*(-\omega, -\mathbf{k})$, guaranteeing the electromagnetic fields are real-valued [45]. Two additional constraints should also be considered for realistic materials: stability at static equilibrium $\mathcal{M}(0, \mathbf{k}) =$

$\bar{\mathcal{M}}(0, \mathbf{k}) > 0$, and the ultraviolet limit $\lim_{\omega \rightarrow \infty} \mathcal{M}(\omega, \mathbf{k}) = \mathbb{1}_3$. Here, $\mathbb{1}_3$ is the 3×3 identity matrix and the limit implies transparency at high frequency $\omega \rightarrow \infty$, as the material cannot respond to sufficiently fast temporal oscillations.

Combining all the above criteria, we find that the response function can always be decomposed as a discrete summation of oscillators [27,30,46],

$$\mathcal{M}(\omega, \mathbf{k}) = \mathbb{1}_3 - \sum_\alpha \frac{C_{\alpha\mathbf{k}}^\dagger C_{\alpha\mathbf{k}}}{\omega_{\alpha\mathbf{k}}(\omega - \omega_{\alpha\mathbf{k}})}. \quad (6)$$

α labels any arbitrary bosonic excitation in the material, such as an exciton or phonon, which couples linearly to the electromagnetic fields via the 3×3 tensor $C_{\alpha\mathbf{k}}$. $\omega_{\alpha\mathbf{k}}$ is the resonant energy of the oscillator and corresponds to a first-order pole of the response function. Note both $C_{\alpha\mathbf{k}}$ and $\omega_{\alpha\mathbf{k}}$ are in general \mathbf{k} dependent. We emphasize that the response function is consistent with previous work on gyrotropic plasmas [47,48]. However, our key advance is that the tensors $C_{\alpha\mathbf{k}}$, characterizing the collective light-matter excitations, carry information of spin and orbital angular momentum.

C. Continuum Hamiltonian

A detailed derivation of the continuum electromagnetic Hamiltonian $H(\mathbf{k})$ is presented in Appendix B. To accomplish this, we expand the response function $\mathcal{M}(\omega, \mathbf{k})$ in terms of three-component matter oscillators ψ_α . These represent internal polarization and magnetization modes of the material,

$$\psi_\alpha = \frac{C_{\alpha\mathbf{k}} f}{\omega - \omega_{\alpha\mathbf{k}}}, \quad \omega \psi_\alpha = \omega_{\alpha\mathbf{k}} \psi_\alpha + C_{\alpha\mathbf{k}} f. \quad (7)$$

We now define u as the generalized state vector of the electromagnetic problem, accounting for the photon f and all possible internal excitations ψ_α ,

$$H(\mathbf{k})u = \omega u, \quad u = [f \quad \psi_1 \quad \psi_2 \quad \dots]^\top, \quad (8)$$

which satisfies a first-order Hamiltonian wave equation. Notice that contraction of u naturally reproduces the energy density upon summation over all degrees of freedom $u^\dagger u = f^\dagger \bar{\mathcal{M}} f$, with $\bar{\mathcal{M}} = \partial_\omega(\omega\mathcal{M}) > 0$ always positive definite. The continuum Hamiltonian $H(\mathbf{k})$ acting on u is given concisely

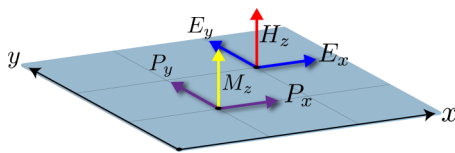


FIG. 2. Only transverse-magnetic (TM) waves propagate as charge is restricted to the x - y plane (blue and red arrows denote the fields). This limits the degrees of freedom of both the electromagnetic field and the induced response of a material. Electromagnetic polarization and magnetization response in a 2D material is shown with the purple and yellow arrows. The electric and magnetic displacement fields are the linear superposition of $D_i = P_i + E_i$ and $B_z = M_z + H_z$. Our focus in this paper is gyrotropic media which correspond to optical (dynamical) Hall conductivity.

as

$$H(\mathbf{k}) = \begin{bmatrix} \mathcal{H}_0(\mathbf{k}) + \sum_{\alpha} \omega_{\alpha\mathbf{k}}^{-1} C_{\alpha\mathbf{k}}^{\dagger} C_{\alpha\mathbf{k}} & C_{1\mathbf{k}}^{\dagger} & C_{2\mathbf{k}}^{\dagger} & \dots \\ C_{1\mathbf{k}} & \omega_{1\mathbf{k}} & 0 & \dots \\ C_{2\mathbf{k}} & 0 & \omega_{2\mathbf{k}} & \dots \\ \vdots & \vdots & \vdots & \ddots \end{bmatrix}. \quad (9)$$

This eigenvalue problem generates the complete spectrum of quasiparticle eigenstates,

$$H_{\mathbf{k}} u_{n\mathbf{k}} = \omega_{n\mathbf{k}} u_{n\mathbf{k}}, \quad (10)$$

and the eigenstates are normalized to the energy density $u_{n\mathbf{k}}^{\dagger} u_{n\mathbf{k}} = f_{n\mathbf{k}}^{\dagger} \bar{\mathcal{M}}(\omega_{n\mathbf{k}}, \mathbf{k}) f_{n\mathbf{k}} = 1$. Moreover, the eigenenergies $\omega_{n\mathbf{k}}$ are the n nontrivial roots of the characteristic equation,

$$\det[\mathcal{H}_0(\mathbf{k}) - \omega \mathcal{M}(\omega, \mathbf{k})] = 0, \quad \omega = \omega_n(\mathbf{k}), \quad (11)$$

proving that the response function $\mathcal{M}(\omega, \mathbf{k})$ is derived from a first-order Hamiltonian $H(\mathbf{k})$.

D. Continuum regularization (one-point compactification)

Our goal is to develop a continuum topological theory that accounts for both spatiotemporal dispersion and the inherent bosonic properties of light. Due to the unbounded nature of the momentum space \mathbb{R}^2 , continuum Chern numbers are usually ill-defined. Nevertheless, as long as the system is properly *regularized*, continuum field theories are possible and can be incredibly powerful tools to study long-wavelength topological physics [49–51]. A necessary condition is one-point compactification of the momentum space [52–54], which governs the high- k asymptotic behavior of the Hamiltonian. This requirement is well understood in condensed matter and demands the Hamiltonian approach a *directionally independent* value,

$$\lim_{k \rightarrow \infty} H(\mathbf{k}) \rightarrow H(k), \quad (12)$$

where $k = \sqrt{\mathbf{k} \cdot \mathbf{k}}$ is the magnitude of the wave vector. In this way, all limits at infinity are mapped into the same point and satisfy a “periodic” boundary condition. The momentum space is closed and topologically equivalent to the Reimann sphere $\mathbb{R}^2 \simeq S^2$ (Fig. 3). Hence, Chern numbers are quantized. A rigorous proof is presented in Appendix C.

This constraint has important implications in continuum photonic media. Since Maxwell’s equations are strictly first order in spatial derivatives [Eq. (3)], one-point compactification can only be satisfied by introducing nonlocality [55,56]. Nonlocality (or spatial dispersion) is the momentum dependence of linear response—commonly ignored in photonics problems, dc transport measurements, as well as Faraday rotation experiments. However, we strongly emphasize that the high- k behavior cannot be neglected even in the long-wavelength continuum theory. These deep subwavelength components encode global information of the fields and are essential to properly describe the topological physics. By exploiting rotational symmetry, we will show that the asymptotic behavior of the Hamiltonian $H(\mathbf{k})$ and by extension, the response function $\mathcal{M}(\omega, \mathbf{k})$, is naturally regularized and predicts bosonic phases of matter.

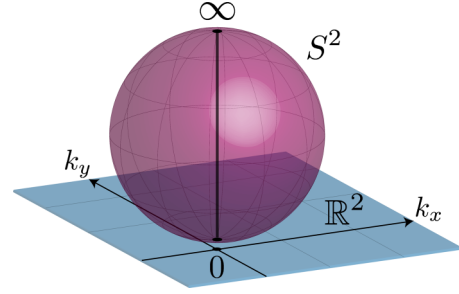


FIG. 3. One-point compactification of the momentum space $\mathbb{R}^2 \simeq S^2$ over which the topological quantum numbers are defined. When the Hamiltonian is properly regularized, the planar \mathbf{k} space is topologically equivalent to the bounded Reimann sphere. $k_p = 0$ and $k_p = \infty$ are the rotationally invariant (high-symmetry) points on the sphere, passing through the z axis. This procedure is necessary to ensure Chern quantization in continuum topological field theories and fundamentally requires nonlocal photonic media.

III. ROTATIONAL SYMMETRY

A. Definition of orbital, spin, and total angular momentum

If the two-dimensional crystal has a center (at least threefold cyclic [57,58]), the continuum Hamiltonian is rotationally symmetric about z ,

$$\mathcal{R}^{-1} H(\mathcal{R}\mathbf{k}) \mathcal{R} = H(\mathbf{k}), \quad \mathcal{R}(2\pi) = \mathbb{1}_3, \quad (13)$$

and the eigenenergies $\omega = \omega_n(k)$ depend only on the magnitude of k . Note that \mathcal{R} is diagonal in u , meaning the photon and each oscillator is rotated individually, $f \rightarrow \mathcal{R}f$ and $\psi_{\alpha} \rightarrow \mathcal{R}\psi_{\alpha}$. In this case $\mathcal{R}(\theta)$ is a continuous rotation,

$$\mathcal{R}(\theta) = \exp[i\theta \hat{S}_z] = \begin{bmatrix} \cos \theta & \sin \theta & 0 \\ -\sin \theta & \cos \theta & 0 \\ 0 & 0 & 1 \end{bmatrix}, \quad (14)$$

and can be expressed as the exponential of the spin-1 generator $(\hat{S}_z)_{ij} = -i\epsilon_{ijz}$. This represents an element of $SO(3)$ in the subspace of \mathbb{R}^2 [59], as all rotations occur in the x - y plane. We stress that the vector representation is *bosonic*, meaning the quasiparticles return in phase under cyclic revolution $\mathcal{R}(2\pi) = \mathbb{1}_3$.

Since the Hamiltonian possesses a *continuous* rotational symmetry, the total angular momentum (TAM) is conserved,

$$[\hat{J}_z, H(\mathbf{k})] = 0, \quad \hat{J}_z = \hat{L}_z + \hat{S}_z. \quad (15)$$

Equations (13) and (15) are equivalent statements in this context. Here, \hat{L}_z is the orbital angular momentum (OAM) operator in 2D \mathbf{k} space and can be expressed in polar coordinates as

$$\hat{L}_z = -ik_x \frac{\partial}{\partial k_y} + ik_y \frac{\partial}{\partial k_x} = -i\partial_{\phi}. \quad (16)$$

Eigenstates of the OAM are well known and represent quantized azimuthal charges,

$$\hat{L}_z |l\rangle = l|l\rangle, \quad |l\rangle = \exp(il\phi), \quad (17)$$

where $l \in \mathbb{Z}$ is any integer.

Conversely, eigenstates of the spin angular momentum (SAM) represent states of quantized polarization, transverse

to the x - y plane,

$$\hat{S}_z \mathbf{e} = m \mathbf{e}. \quad (18)$$

The matrix form of \hat{S}_z is given in Eq. (4). For photons, the spin is an integer $m = \pm 1, 0$ and takes one of three discrete values. First, we have the $m = \pm 1$ spin states,

$$\mathbf{e}_{\pm} = \frac{1}{\sqrt{2}} \begin{bmatrix} 1 \\ \pm i \\ 0 \end{bmatrix}, \quad \hat{S}_z \mathbf{e}_{\pm} = \pm \mathbf{e}_{\pm}. \quad (19)$$

\mathbf{e}_{\pm} are resonant electric ($H_z = 0$) counter-rotating states. Second, we have the $m = 0$ spin state, which is resonant magnetic ($E_i = 0$) and irrotational,

$$\mathbf{e}_0 = \begin{bmatrix} 0 \\ 0 \\ 1 \end{bmatrix}, \quad \hat{S}_z \mathbf{e}_0 = 0. \quad (20)$$

A visualization of the quantized spin-1 states is displayed in Fig. 1(a) and this is compared to quantized spin-1/2 states in Fig. 1(b). In Sec. IV, we will prove that these spin quantized eigenstates naturally arise at high-symmetry \mathbf{k} points in 2+1D bosonic phases.

B. High-symmetry points and gauge singularities

At an arbitrary momentum \mathbf{k} , the quasiparticles $u_{n\mathbf{k}}$ are not eigenstates of \hat{L}_z or \hat{S}_z . Instead, they are eigenstates of the total angular momentum $\hat{J}_z = \hat{L}_z + \hat{S}_z$,

$$\hat{J}_z u_{n\mathbf{k}} = j_n u_{n\mathbf{k}}, \quad j_n \in \mathbb{Z}, \quad (21)$$

where j_n is an integer for bosons. Since \hat{J}_z is a differential operator, the choice of j_n represents a particular Berry gauge for the eigenstates. This gauge is single-valued for all \mathbf{k} with the possible exception of two points, $k_p = 0$ and $k_p = \infty$. These are called *high-symmetry points* (HSPs). At these specific momenta, the Hamiltonian is *rotationally invariant* [60],

$$\mathcal{R}^{-1} H(k_p) \mathcal{R} = H(k_p), \quad [\hat{S}_z, H(k_p)] = 0, \quad (22)$$

which follows immediately from Eqs. (13) and (15). In the continuum theory, $k_p = 0$ is a HSP because the origin always rotates into itself. Owing to one-point compactification [Eq. (12)], $k_p = \infty$ is also a HSP. This is clear by direct inspection of the Riemann sphere in Fig. 3. A rotation in the plane of \mathbb{R}^2 rotates S^2 about its axis, keeping both $k_p = 0$ and $k_p = \infty$ fixed. Invariance at $k_p = \infty$ is therefore imperative to describe continuum topological theories.

At HSPs the SAM of any eigenstate $u_{n\mathbf{k}}$ is quantized and this is guaranteed by symmetry [Eq. (22)]. Still, the Berry gauge may be multivalued here due to the OAM—known as a phase singularity [61],

$$\lim_{\mathbf{k} \rightarrow k_p} u_n(\mathbf{k}) \rightarrow u_n(k_p) \exp[i l_n(k_p) \phi], \quad (23)$$

$$\hat{S}_z u_n(k_p) = m_n(k_p) u_n(k_p), \quad (24)$$

where $j_n = l_n(k_p) + m_n(k_p)$ at HSPs. We come to an important revelation from Eq. (23). If the spin *does not change* within the eigenstate dispersion $m_n(0) = m_n(\infty)$, we can remove the phase singularity at both points simultaneously, $l_n(0) =$

$l_n(\infty) = 0$, such that the Berry gauge $j_n = m_n(0) = m_n(\infty)$ is single-valued for all \mathbf{k} .

However, if the spin *changes* within the dispersion $m_n(0) \neq m_n(\infty)$, this procedure is impossible. The Berry gauge is always multivalued because the singularity $l_n(k_p) \neq 0$ cannot be resolved at $k_p = 0$ and $k_p = \infty$ simultaneously. This is a nontrivial topology. The physical interpretation is simple but profound; since the TAM is conserved for each eigenstate $\Delta j_n = 0$, the OAM $\Delta l_n = l_n(\infty) - l_n(0) \neq 0$ must change to compensate for the SAM,

$$\Delta l_n = -\Delta m_n = m_n(0) - m_n(\infty). \quad (25)$$

We will now prove that Eq. (25) fundamentally defines the Chern classification of 2+1D bosonic phases.

IV. CONTINUUM TOPOLOGICAL BOSONIC PHASES

A. Continuum photonic Chern number

Utilizing the eigenstates of the Hamiltonian in Eq. (10), we obtain the Berry connection by varying a quasiparticle with respect to the momentum,

$$\mathbf{A}_n(\mathbf{k}) = -i u_{n\mathbf{k}}^\dagger \partial_{\mathbf{k}} u_{n\mathbf{k}}. \quad (26)$$

Applying the curl produces the gauge invariant Berry curvature $F_n(\mathbf{k}) = \hat{\mathbf{z}} \cdot [\partial_{\mathbf{k}} \times \mathbf{A}_n(\mathbf{k})]$. The Chern number C_n is a global topological invariant and is traditionally found by integrating F_n over the 2D Brillouin zone—i.e., the torus $\mathbb{T}^2 = S^1 \times S^1$. For continuum theories, we integrate over the entire 2D momentum space \mathbb{R}^2 ,

$$C_n = \frac{1}{2\pi} \iint_{\mathbb{R}^2} F_n(\mathbf{k}) d^2\mathbf{k}. \quad (27)$$

When properly regularized, the planar manifold is topologically equivalent to the Riemann sphere $\mathbb{R}^2 \simeq S^2$ and the Chern number is quantized (Appendix C).

Although photonic Chern numbers have been defined, neither the high- k behavior nor the inherent bosonic properties have been addressed. With this in mind, we return to the Berry connection \mathbf{A}_n in polar coordinates $\partial_{\mathbf{k}} = \hat{\mathbf{k}} \partial_k + \hat{\phi} \partial_\phi$,

$$\mathbf{A}_n(\mathbf{k}) = \hat{\mathbf{k}} A_n^k(k) + \hat{\phi} A_n^\phi(k). \quad (28)$$

Due to rotational symmetry, the polar components of \mathbf{A}_n depend only on k . Furthermore, we can connect the Berry potential A_n^ϕ directly to the OAM,

$$A_n^\phi(k) = -i u_{n\mathbf{k}}^\dagger \partial_\phi u_{n\mathbf{k}} = \langle \hat{L}_z \rangle_n. \quad (29)$$

Here, $\langle \hat{L}_z \rangle_n$ is the expectation value of the OAM for the n th eigenstate. This corresponds to a Berry curvature F_n of

$$F_n(k) = \partial_k \langle \hat{L}_z \rangle_n. \quad (30)$$

When integrating over all momenta $d^2\mathbf{k} = dk d\phi$, we find that the continuum Chern number C_n is determined solely by the phase singularities at HSPs,

$$C_n = \int_0^\infty dk \partial_k \langle \hat{L}_z \rangle_n = \langle \hat{L}_z \rangle_n \Big|_0^\infty = \Delta l_n, \quad (31)$$

precisely the change in OAM. Substituting for $\Delta l_n = -\Delta m_n$ in Eq. (25), we attain an elegant expression for the Chern number,

$$C_n = \Delta l_n = m_n(0) - m_n(\infty). \quad (32)$$

Equation (32) is one of the central results of this paper and is valid for both fermionic and bosonic representations. Essential differences between the two are immediately apparent.

For a spin-1/2 electron, quanta take one of two half-integer values, $m_n = \pm \frac{1}{2}$. Consequently, we find only one truly distinct fermionic phase,

$$\text{fermion: } C_n = \pm 1, 0. \quad (33)$$

However, for the spin-1 photon, quanta take three integer values $m_n = \pm 1, 0$. We discover two unique bosonic phases,

$$\text{boson: } C_n = \pm 2, \pm 1, 0. \quad (34)$$

One with even parity $C_n = \pm 2$ and one with odd $C_n = \pm 1$. Even parity corresponds to a change from $m_n(0) = \pm 1$ to $m_n(\infty) = \mp 1$ at HSPs. This phase is familiar in interacting bosonic systems and is identified with a *single* gapless boson at the edge [8–13]—not two as we might expect from fermionic Chern number arguments. Odd parity bosonic phases are quite exotic in this regard [62,63]. This phase corresponds to a change from $m_n(0) = \{0, \pm 1\}$ to $m_n(\infty) = \{\pm 1, 0\}$ at HSPs.

B. Nonlocal regularization of the response function

We now derive the asymptotic behavior of the Hamiltonian $H(\mathbf{k})$ to ensure the continuum theory is properly regularized at $k \rightarrow \infty$. This will help us discover the precise form of the response function $\mathcal{M}(\omega, \mathbf{k})$ and the order of nonlocality necessary to describe a topological field theory. Nonlocality plays two equally important roles in this context—it distinguishes between *trivial* and *nontrivial* phases. If high- k components are ignored, it is impossible to define either of these phases in the continuum.

From Eqs. (6) and (9), rotational symmetry implies the coupling tensors obey $\mathcal{R}^{-1}C_\alpha(\mathcal{R}\mathbf{k})\mathcal{R} = C_\alpha(\mathbf{k})$ and the oscillator resonances $\omega_\alpha(k)$ depend only on k . We find the exact expression of $C_\alpha(\mathbf{k})$,

$$C_\alpha(\mathbf{k}) = c_\alpha(k)\mathbf{k} \otimes \mathbf{k} + d_\alpha(k)\mathbf{k} \cdot \mathbf{S} + \mathcal{G}_\alpha(k), \quad (35)$$

where $c_\alpha(k)$ and $d_\alpha(k)$ are scalars. It is easy to check that the tensors also commute with $[\hat{J}_z, C_\alpha(\mathbf{k})] = 0$, conserving TAM. $c_\alpha(k)$ introduces a nonlocal birefringence in ε_{ij} and $d_\alpha(k)$ is a type of nonlocal magnetoelectricity χ_i . Both terms are permitted by symmetry but neither is important, as all contributions besides $\mathcal{G}_\alpha(k)$ vanish identically at $k_p = 0$ and $k_p = \infty$. This is because $\mathcal{G}_\alpha(k)$ is the only rotationally invariant component of $C_\alpha(\mathbf{k})$, which defines the topology,

$$\mathcal{R}^{-1}\mathcal{G}_\alpha(k)\mathcal{R} = \mathcal{G}_\alpha(k), \quad [\hat{S}_z, \mathcal{G}_\alpha(k)] = 0. \quad (36)$$

The Hamiltonian in Eq. (9) takes the following form at HSPs:

$$H(k_p) = \begin{bmatrix} \sum_\alpha \omega_{\alpha k_p}^{-1} \mathcal{G}_{\alpha k_p}^\dagger \mathcal{G}_{\alpha k_p} & \mathcal{G}_{1k_p}^\dagger & \mathcal{G}_{2k_p}^\dagger & \dots \\ \mathcal{G}_{1k_p} & \omega_{1k_p} & 0 & \dots \\ \mathcal{G}_{2k_p} & 0 & \omega_{2k_p} & \dots \\ \vdots & \vdots & \vdots & \ddots \end{bmatrix}. \quad (37)$$

Notice the vacuum Maxwell equations $\mathcal{H}_0(\mathbf{k})$ play no role in either limit; the Hamiltonian is governed entirely by the material response at HSPs. Nevertheless, this imposes pivotal

stipulations on the asymptotic behavior. The largest powers in k must arise from $\mathcal{G}_{\alpha k}$ as these terms dominate at exceedingly large momentum $k \rightarrow \infty$. Consequently, $\mathcal{G}_{\alpha k}$ and $\omega_{\alpha k}$ require quadratic nonlocality $\propto k^2$ at *minimum*, since the vacuum fields $\mathcal{H}_0(\mathbf{k})$, which are linear in \mathbf{k} , must be outpaced in the $k \rightarrow \infty$ limit.

By extension of Eq. (37), the response function is regularized and rotationally invariant at HSPs,

$$[\hat{S}_z, \mathcal{M}(\omega, k_p)] = 0. \quad (38)$$

Upon summation over all oscillators describing the linear response, \mathcal{M} takes a remarkably simple form,

$$\begin{aligned} \mathcal{M}(\omega, k_p) &= \mathbb{1}_3 - \sum_\alpha \frac{\mathcal{G}_{\alpha k_p}^\dagger \mathcal{G}_{\alpha k_p}}{\omega_{\alpha k_p}(\omega - \omega_{\alpha k_p})} \\ &= \begin{bmatrix} \varepsilon & ig & 0 \\ -ig & \varepsilon & 0 \\ 0 & 0 & \mu \end{bmatrix}, \end{aligned} \quad (39)$$

where all parameters are evaluated at k_p . Here, ε and μ are the conventional scalar permittivity and permeability of a 2D material. g is a generalized gyrotropic coupling which breaks both parity and time-reversal symmetry.

Although the condition at $k_p = \infty$ is a mathematical requisite, it makes perfect sense physically when we acknowledge that the continuum theory is simply an approximation of the underlying crystal lattice. In reality, the momentum can never reach arbitrarily large values. As the momentum approaches the scale of the lattice constant $ka \approx \pi$, the wave approaches a Bragg condition. These are HSPs in the reciprocal lattice [57–60] so the continuum theory must encode this behavior. Accordingly, the $k \rightarrow \infty$ limit should be interpreted as a Bragg resonance.

C. Transverse spin quantization of the photon

We go one step further to uncover the precise origin of the spin-1 eigenvalues $m_n(k_p)$, the spin states \mathbf{e} , and their relation to the response function \mathcal{M} . At HSPs, the SAM expectation value is represented as

$$\langle \hat{S}_z \rangle_n = m_n(k_p) = u_n^\dagger(k_p) \hat{S}_z u_n(k_p). \quad (40)$$

Using Eqs. (7) and (36), this can be simplified to yield

$$m_n(k_p) = f_n^\dagger(k_p) \bar{\mathcal{M}}(\omega_n(k_p), k_p) \hat{S}_z f_n(k_p). \quad (41)$$

We note that precisely at HSPs, the quantum of spin $m_n(k_p)$ is determined entirely by the photonic component $f_n(k_p)$ of the eigenmode $u_n(k_p)$ —but not the coordinates of the matter oscillations ψ_α . Utilizing the normalization condition $f_n^\dagger(k_p) \bar{\mathcal{M}}(\omega_n(k_p), k_p) f_n(k_p) = 1$, Eq. (41) leads to

$$\hat{S}_z f_n(k_p) = m_n(k_p) f_n(k_p). \quad (42)$$

This indicates that the electromagnetic wave function f must be a spin state $f_n(k_p) \propto \mathbf{e}$ at HSPs [Eq. (18)].

Our problem reduces to finding the eigenstates of the photon at HSPs and directly evaluating their spin eigenvalues. We return to the characteristic equation in Eq. (11), which defines the photonic wave function f . As $k \rightarrow 0$, the vacuum equations vanish identically, $\mathcal{H}_0(\mathbf{k}) \rightarrow 0$. Moreover, the response

function is regularized and includes quadratic nonlocality $\propto k^2$ at minimum. As $k \rightarrow \infty$, the vacuum fields do not contribute $\mathcal{H}_0(\mathbf{k}) \rightarrow 0$. Therefore, a nontrivial solution exists $\omega_n(k_p) \neq 0$ if and only if it satisfies

$$\det[\mathcal{M}(\omega_n(k_p), k_p)] = 0. \quad (43)$$

Equation (43) represents the threshold condition at $k_p = 0$ and the Bragg condition at $k_p = \infty$ for any particular eigenstate n . To allow for nontrivial solutions $\mathcal{M}f = 0$ in Eq. (39), one of three possible conditions must be fulfilled,

$$\frac{g(\omega_n(k_p), k_p)}{\varepsilon(\omega_n(k_p), k_p)} = \pm 1, \quad \text{or} \quad \mu(\omega_n(k_p), k_p) = 0. \quad (44)$$

We see that the photonic wave function is clearly a spin-1 eigenstate $f_n(k_p) \propto \mathbf{e}$ at HSPs. The gyrotropic constraint gives us counter-rotating spin states $\hat{S}_z \mathbf{e}_{\pm} = \pm \mathbf{e}_{\pm}$ with eigenvalues $m_n(k_p) = \pm 1$, while the magnetic constraint gives us the irrotational spin state $\hat{S}_z \mathbf{e}_0 = 0$ with eigenvalue $m_n(k_p) = 0$. Physically, these conditions at HSPs correspond to gyrotropic or magnetic plasmon resonances in the bulk 2D material. In a lattice theory, the resonance at $k_p = 0$ describes the response at the Γ point, while $k_p = \infty$ describes the behavior near the edges of the Brillouin zone.

The meaning behind each topological bosonic phase is now revealed. In the even parity phase $C_n = \pm 2$, a gyrotropic mode dominates but the handedness of the plasmon changes at HSPs, $g/\varepsilon = \pm 1 \rightarrow \mp 1$. If the handedness does not change as $k \rightarrow \infty$, the phase is trivial $C_n = 0$. The odd parity phase $C_n = \pm 1$ is very different however. Instead, the mode changes from a magnetic plasmon $\mu = 0$ to a gyrotropic plasmon $g/\varepsilon = \pm 1$ at HSPs. In the following sections, we restrict our discussion to the even parity phase $C_n = \pm 2$. The odd parity phase $C_n = \pm 1$ is significantly more complicated and will be dedicated to a future paper.

D. Even parity bosonic phase: $C = \pm 2$

We adopt an exactly solvable model to unravel the low-energy topological physics of this phase. We let the response function be rotationally invariant $[\hat{S}_z, \mathcal{M}(\omega, k)] = 0$ at all momenta, while also assuming $\varepsilon = \text{const} > 1$ is dielectric and the response is nonmagnetic $\mu = 1$. In this case, all the physics is captured by the gyrotropic coefficient g , which is the high-frequency analog of the dc Hall conductivity,

$$g(\omega, k) = \frac{\sigma_H(k)}{\omega}, \quad \sigma_H(k) = \sigma_0 - \sigma_2(ka)^2. \quad (45)$$

$\sigma_H(k)$ is a nonlocal Hall conductivity [64]. σ_0 is the static response and σ_2 characterizes the momentum dependence (scaled to the lattice constant a). At low energy $\omega \rightarrow 0$, this is the only admissible form of $g \neq 0$ [47,48]. Due to the reality of the electromagnetic field $\mathcal{M}^*(-\omega, k) = \mathcal{M}(\omega, k)$, gyrotropy must always be odd in frequency $g(-\omega, k) = -g(\omega, k)$. This means a first-order pole at $\omega = 0$ is permissible and corresponds to nonzero Hall conductivity $\omega g(\omega, k) = \sigma_H(k) \neq 0$. The energy density is positive definite $\bar{\mathcal{M}} = \partial_\omega(\omega \mathcal{M}) = \text{diag}[\varepsilon, \varepsilon, 1] > 0$ and nonsingular at $\omega = 0$.

We highlight important aspects of our model and the connections to experimentally measured gyrotropic responses. First, we deal with Hermitian systems so the imaginary

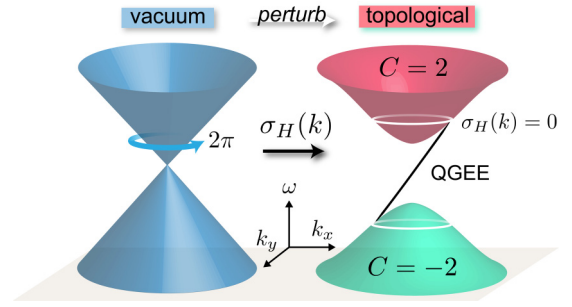


FIG. 4. Schematic of the exactly solvable topological model. In vacuum, Maxwell's equations can be written in the form $\mathcal{H}_0(\mathbf{k}) = \mathbf{k} \cdot \mathbf{S}$, which captures both the spin-1 behavior and linear dispersion of the massless photon. The gyrotropic medium perturbs the linear dispersion and induces a bulk band gap near zero frequency. In this case, the perturbation is a nonlocal Hall conductivity $\sigma_H(k) = \sigma_0 - \sigma_2(ka)^2$, which behaves identically to the effective mass of the Dirac equation. If $\sigma_H(k) = 0$ passes through zero at some finite momentum, the medium is topological. The nontrivial phase $C = 2$ corresponds to a gapless unidirectional photon at the boundary, dubbed the quantum gyroelectric effect (QGEE). We strongly emphasize that this model is validated by direct comparison with the supersymmetric Dirac theory for continuum fermions.

part of the dielectric permittivity is zero $\text{Im}[\varepsilon] = \sigma/\omega = 0$. Therefore, no dissipative currents exist in this system and the gyrotropic coefficient is related only to a dissipationless Hall current. Experimentally measured variables connecting to the gyrotropic coefficient, such as Verdet constants, are highly frequency dependent and this is consistent with our model. Furthermore, the zero frequency behavior of the gyrotropic coefficient $g = \sigma_H/\omega$ is in agreement with first-order poles in standard models of conductivity $\text{Im}[\varepsilon] = \sigma/\omega$.

Remarkably, the quadratic spatial correction to σ_H is sufficient to describe a topological photonic phase and the continuum theory is regularized at $k \rightarrow \infty$. The interpretation is particularly simple in this context. At long wavelengths $\sigma_H(k \rightarrow 0) \rightarrow \sigma_0$, the Hall conductivity induces circulating currents of a specific handedness (clockwise or counterclockwise), but at short wavelengths $\sigma_H(k \rightarrow \infty) \rightarrow -\sigma_2(ka)^2$, the handedness can reverse directions. We will show that when σ_H switches sign, the phase is nontrivial.

E. Bulk (bosonic Chern insulator)

In vacuum, the photon is massless and therefore linearly dispersing $\omega = k$. This is the photonic (spin-1) equivalent of a Dirac point and arises naturally from Maxwell's equations $\mathcal{H}_0(\mathbf{k}) = \mathbf{k} \cdot \mathbf{S} = k_x \hat{S}_x + k_y \hat{S}_y$, as mentioned in Sec. II. By introducing the Hall conductivity, the linear dispersion of bulk waves fundamentally changes—a gap is formed at zero frequency $\omega = 0$,

$$\varepsilon \omega^2(k) = k^2 + \frac{\sigma_H^2(k)}{\varepsilon}, \quad (46)$$

where σ_H acts identically to an effective photon mass [41,42]. ε governs the effective speed of light. A schematic of the vacuum and bulk dispersion is displayed in Fig. 4.

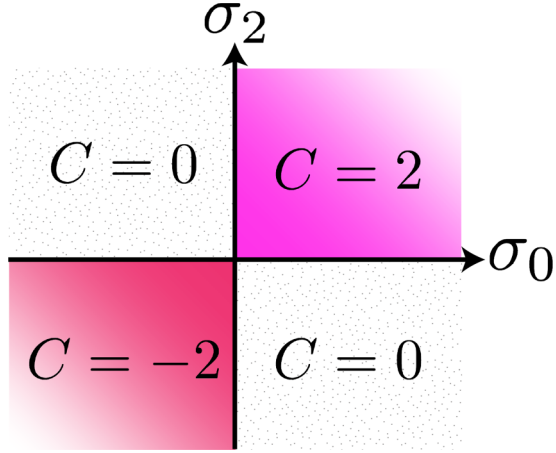


FIG. 5. Topological phase diagram of the nonlocal Hall model $\sigma_H(k) = \sigma_0 - \sigma_2(ka)^2$. $C = \text{sgn}[\sigma_0] + \text{sgn}[\sigma_2]$ corresponds to the Chern number of the positive frequency band $\omega > 0$. The Chern number of the negative frequency band $\omega < 0$ is exactly opposite $-C$. When $\sigma_0\sigma_2 > 0$, the photon is in a nontrivial bosonic phase $C = \pm 2$, while $\sigma_0\sigma_2 < 0$ is a trivial phase $C = 0$. In the continuum theory, trivial and nontrivial phases can only be distinguished by incorporating nonlocality $\sigma_2 \neq 0$.

There is only one positive frequency $\omega > 0$ eigenstate associated with this system and is expressed in polar coordinates as

$$f_{\mathbf{k}} = \begin{bmatrix} E_x \\ E_y \\ H_z \end{bmatrix} = \frac{1}{\sqrt{2\varepsilon}} \left(\frac{\sigma_H}{\varepsilon\omega} \hat{\mathbf{k}} + i\hat{\boldsymbol{\phi}} + i\frac{k}{\omega} \hat{\mathbf{z}} \right) e^{i\phi}. \quad (47)$$

$f_{\mathbf{k}}$ is normalized to the energy density $1 = f_{\mathbf{k}}^\dagger \bar{\mathcal{M}} f_{\mathbf{k}}$ and is written in a fixed Berry gauge defined by the TAM $\hat{J}_z f_{\mathbf{k}} = f_{\mathbf{k}}$. We now show that the photon in this eigenstate exhibits transverse spin quantization at HSPs, which is independent of the chosen Berry gauge. From Eq. (47) above, we have $\hat{S}_z f(k_p) = m(k_p) f(k_p)$ at the plasmon resonances,

$$m(k_p) = \frac{g(\omega(k_p), k_p)}{\varepsilon(\omega(k_p), k_p)} = \frac{\sigma_H(k_p)}{\varepsilon\omega(k_p)} = \text{sgn}[\sigma_H(k_p)]. \quad (48)$$

Since ε is a constant, the eigenvalues are determined solely by the long- and short-wavelength behavior of the Hall conductivity, $m(0) = \text{sgn}[\sigma_0]$ and $m(\infty) = -\text{sgn}[\sigma_2]$, giving a Chern number of

$$C = m(0) - m(\infty) = \text{sgn}[\sigma_0] + \text{sgn}[\sigma_2]. \quad (49)$$

A nontrivial phase corresponds to $\sigma_0\sigma_2 > 0$, which can be $C = \pm 2$ depending on the signs of σ_0 and σ_2 . This is the simplest realization of a bosonic Chern insulator [65]. It is equally important to note that $\sigma_0\sigma_2 < 0$ corresponds to a trivial phase $C = 0$. Distinguishing between trivial $C = 0$ and nontrivial $C = \pm 2$ phases is only possible by incorporating nonlocality $\sigma_2 \neq 0$. A topological phase diagram of this system is presented in Fig. 5.

In the nontrivial phase, there is a point where the Hall conductivity $\sigma_H(k) = 0$ passes through zero—precisely at $ka = \sqrt{\sigma_0/\sigma_2}$. The zero must occur for the spin to change handedness and can only be removed by a topological phase transition. This also puts an approximate bound on the Hall

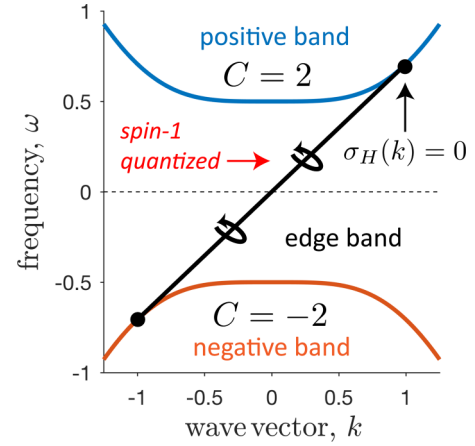


FIG. 6. Continuum band diagram $\omega(k)$ of the even parity $C = 2$ topological bosonic phase. The negative frequency branch has a Chern number of -2 ; necessary for the total summation to vanish $2 - 2 = 0$. As an example, we have let $\sigma_0 = \sigma_2 a^2 = 1$ and $\varepsilon = 2$. The unidirectional edge state is spin-1 helically quantized and touches the bulk bands precisely where the nonlocal Hall conductivity passes through zero $\sigma_H(k) = 0$. At this point $ka = \sqrt{\sigma_0/\sigma_2}$, the edge state joins the continuum of bulk bands. Notice that no edge solution exists for $k_y \rightarrow -k_y$ and the photon is immune to backscattering.

parameters. As long as $\sqrt{\sigma_0/\sigma_2} \ll \pi$ the continuum theory is valid and the zero occurs within the Brillouin zone. As an aside, we note the negative frequency band $\omega < 0$ has a Chern number of $-C$ —exactly the opposite of the positive band. This is necessary to ensure the summation over all bands vanishes, $\sum_n C_n = 0$.

F. Edge (quantum gyroelectric effect)

Finally, we analyze the unique edge state of this bosonic phase, which has no counterpart in traditional surface photonics—such as plasmon polaritons, Tamm states, Dyakonov or Zenneck waves [66]. This is because topological boundary conditions are captured by nonlocal (spatially and temporally dispersive) optical constants. In conventional problems, nonlocality introduces additional boundary conditions (ABCs) [55,67] which need to be satisfied to uniquely determine the electromagnetic field. The photonic edge state discussed here is fundamentally different in this context. The behavior of the field outside the medium $x < 0$ becomes irrelevant due to topological *open boundary conditions* $f(x = 0^+) = 0$ [49–51,68]. Open boundary conditions are commonly encountered in topological electronics [69,70] but is surprising when dealing with photons. To be localized at the edge, all components of the field must decay into the bulk $f(x = \infty) = 0$ as $x \rightarrow \infty$ and simultaneously disappear on the edge. The exact bulk and edge dispersion is plotted in Fig. 6 and a diagram of the topological edge state is displayed in Fig. 7(a). We strongly emphasize that these special solutions point to the first unified topological theory of Maxwell bosons and Dirac fermions.

The specific phase $C = \pm 2$ will determine if the unidirectional photon is forward or backward propagating; forward for $C = 2$ and backward for $C = -2$. We stress again that

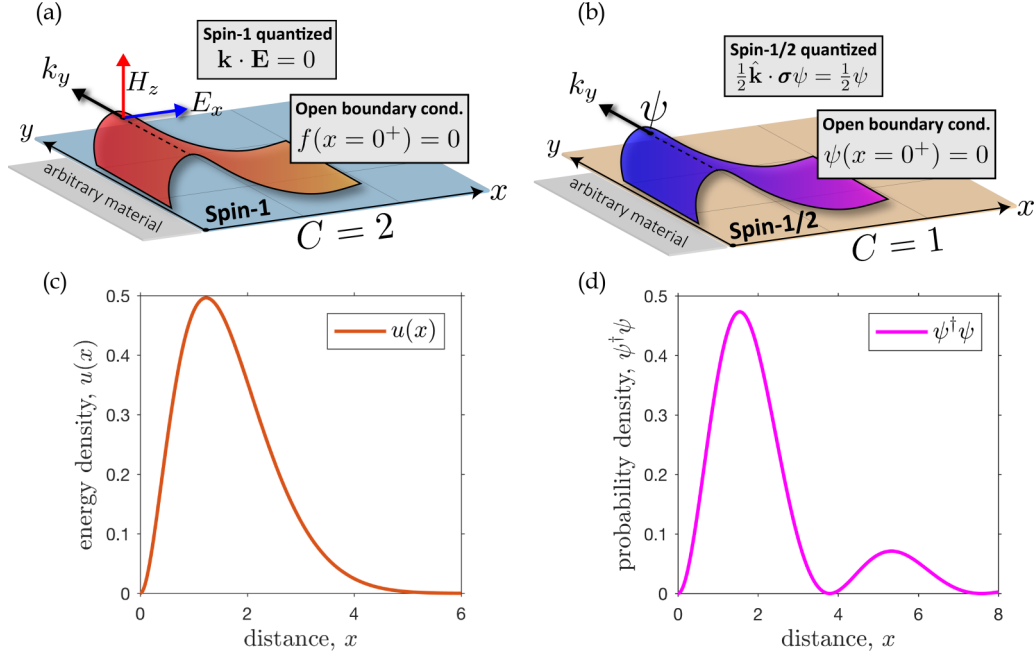


FIG. 7. (a) Topological edge state of the even parity $C = 2$ bosonic phase. The photon is spin-1 helically quantized $\mathbf{k} \cdot \mathbf{E} = 0$ and satisfies open boundary conditions at the interface $f(x = 0^+) = 0$. This ensures the edge state is immune to boundary defects and can exist at any interface—even vacuum. (b) Topological edge state of the $C = 1$ fermionic phase. Like the photon, the electron is spin-1/2 helically quantized $\frac{1}{2}\hat{\mathbf{k}} \cdot \boldsymbol{\sigma}\psi = \frac{1}{2}\psi$ and satisfies open boundary conditions $\psi(x = 0^+) = 0$. (c) Normalized energy density $u(x) = f^\dagger \mathcal{M} f$ of the unidirectional photon as a function of distance x , at a momentum of $k_y = 0.5$. As an example we have let $\sigma_0 = \sigma_2 a^2 = 1$ and $\varepsilon = 2$. Notice the fields are identically zero at $x = 0$ and the edge state exists at the boundary of any interface. (d) Probability density $\psi^\dagger \psi$ of the electronic edge state, where we have let $\Lambda_0 = \Lambda_2 a^2 = 1$ and $v = 0.5$ as an example. The probability density is evaluated for a momentum of $k_y = 0.5$.

for either $C = \pm 2$, there is only one bosonic solution at the boundary—not two. In either case, the solution in the $x > 0$ half space has a similar form $f_\pm(x, y) = f_\pm(x)e^{ik_y y}$. Inserting into the wave equation and applying open boundary conditions, the topological edge state emerges,

$$\omega_\pm = \pm \frac{k_y}{\sqrt{\varepsilon}}, \quad -\sqrt{\frac{\sigma_0}{\sigma_2}} < k_y a < \sqrt{\frac{\sigma_0}{\sigma_2}}, \quad (50a)$$

$$f_\pm(x) = \begin{bmatrix} E_x \\ E_y \\ H_z \end{bmatrix}_\pm = f_0(\hat{\mathbf{x}} \mp \sqrt{\varepsilon} \hat{\mathbf{z}})(e^{-\eta_1 x} - e^{-\eta_2 x}). \quad (50b)$$

A solution only exists in the nontrivial phase $\sigma_0 \sigma_2 > 0$, confirming our theory. Notice the group velocity $v_\pm = \partial \omega_\pm / \partial k_y = \pm 1 / \sqrt{\varepsilon}$ is constant and the edge state can propagate in opposite directions depending on the phase $C = \pm 2$. Moreover, since no solution exists for $k_y \rightarrow -k_y$, the photon is immune to backscattering. The decay lengths η_1 and η_2 are found from the two quadratic roots,

$$\eta_{1,2} = \frac{1}{2a^2|\sigma_2|} \{ \sqrt{\varepsilon} \pm \sqrt{\varepsilon + 4\sigma_2 a^2 [\sigma_2 (k_y a)^2 - \sigma_0]} \}, \quad (51)$$

which determine the degree of confinement at a particular wave vector k_y . A plot of the electromagnetic energy density is presented in Fig. 7(c). Intriguingly, the field is completely transverse polarized $\hat{\mathbf{k}} \cdot \mathbf{E} = E_y = 0$ and helically quantized

along the direction of momentum k_y ,

$$\frac{f_\pm^\dagger \hat{S}_y f_\pm}{f_\pm^\dagger \mathcal{M} f_\pm} = v_\pm = \pm \frac{1}{\sqrt{\varepsilon}}. \quad (52)$$

$\hat{\mathbf{k}} \cdot \mathbf{S} = \hat{S}_y$ is the spin-1 helicity operator and quantization lies in the x - y plane. Consequently, the $C = 2$ phase corresponds to a massless (linearly dispersing) “spin-up” photon while the $C = -2$ phase is a counterpropagating “spin-down” photon. Note that the edge wave is \hat{S}_y helically quantized for *all momenta* and is distinct from transverse \hat{S}_z quantization of the bulk waves, which only occurs at HSPs.

G. Anomalous displacement currents

We also discover an anomalous edge current [71] propagating parallel to the interface,

$$J_y(x, y) = \mp \sqrt{\varepsilon} f_0 (\eta_1 e^{-\eta_1 x} - \eta_2 e^{-\eta_2 x}) e^{ik_y y}. \quad (53)$$

The displacement current is induced by the nonlocal Hall conductivity,

$$J_y = -\partial_x H_z = -(\sigma_0 + \sigma_2 a^2 \nabla^2) E_x, \quad (54)$$

and is highly conductive near the interface $J_y(x=0^+) \neq 0$. However, a compensating current is generated in the bulk $x > 0$, such that the total induced charge is identically zero $\int_{0^+}^{\infty} J_y(x) dx = H_z(0^+) - H_z(\infty) = 0$. Notice that charge neutrality is only guaranteed by the open boundary condition $H_z(x=0^+) = 0$, providing a profound physical basis for

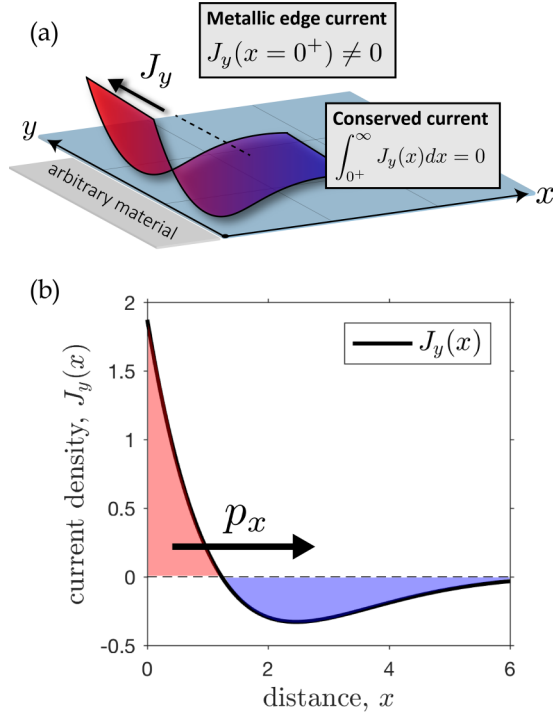


FIG. 8. (a) Anomalous displacement current at the edge of the topological photonic medium. (b) Real current density $J_y(x)$ as a function of distance x , for a momentum of $k_y = 0.5$. We have let $\sigma_0 = \sigma_2 a^2 = 1$ and $\varepsilon = 2$ as an example. The displacement current is generated by the nonlocal Hall conductivity and is highly metallic near the interface $J_y(x = 0^+) \neq 0$. However, the total current is conserved $\int_{0^+}^{\infty} J_y(x) dx = 0$ which is clear from the positive (red) and negative (blue) charge density. Since the net charge is zero, this phenomenon can be interpreted as a propagating dipole bound to the edge of the material—with an intrinsic dipole moment $p_x = \int_{0^+}^{\infty} x \rho(x) dx$.

topological protection. The photonic edge state must exist if the medium is to remain neutral—there is no other option.

From the continuity equation $\omega \rho = k_y J_y$, this phenomenon can also be interpreted as a propagating dipole bound to the edge of the material,

$$p_x = \int_{0^+}^{\infty} x \rho(x) dx = -\varepsilon \int_{0^+}^{\infty} E_x(x) dx = \varepsilon f_0 (\eta_1^{-1} - \eta_2^{-1}), \quad (55)$$

with an intrinsic dipole moment p_x normal to the interface. The intriguing connection to the parity anomaly will be discussed in a future paper [72,73]. The dipole is continuous $x\rho(x)$ and shields the electromagnetic field between regions of positive and negative charge density. This unusual effect allows highly confined photons to propagate at the boundary unimpeded, impervious to defects. A visualization of the anomalous current is displayed in Fig. 8.

V. DIRAC-MAXWELL SUPERSYMMETRY: DIRECT CORRESPONDENCE BETWEEN FERMIONIC AND BOSONIC PHASES

To validate our predictions of the Maxwell theory, we solve the equivalent continuum Dirac theory. These results present a

unified topological field theory of Maxwell-bosons and Dirac-fermions. It also highlights the one-to-one correspondence between even parity bosonic phases $C = \pm 2$ and traditional fermionic phases $C = \pm 1$. Interestingly, the equivalent 2D Dirac theory is a supersymmetric partner of the 2D Maxwell theory [41–44]. The continuum Dirac Hamiltonian is given succinctly as

$$H(\mathbf{k}) = v(k_x \sigma_x + k_y \sigma_y) + \Lambda(k) \sigma_z, \quad (56)$$

where σ_i are the SU(2) Pauli matrices. The dispersion relation of the positive energy state $E > 0$ is found as

$$E^2(k) = v^2 k^2 + \Lambda^2(k), \quad (57)$$

and $\Lambda(k) = \Lambda_0 - \Lambda_2 (ka)^2$ is a spatially dispersive Dirac mass [49–51], v being the Fermi velocity. Again, we include quadratic k dependence for proper regularization at $k \rightarrow \infty$. This direct correspondence makes our earlier claim, the necessity of nonlocality (momentum dependence), very clear.

The Hamiltonian possesses rotational symmetry, which is generated by the spin-1/2 operator $\hat{S}_z = \frac{1}{2} \sigma_z$. This is evidently a fermionic representation $\mathcal{R}(2\pi) = \exp[i2\pi \hat{S}_z] = -\mathbb{1}_2$. Furthermore, we can prove transverse spin-1/2 quantization at HSPs, $m(0) = \frac{1}{2} \text{sgn}[\Lambda_0]$ and $m(\infty) = -\frac{1}{2} \text{sgn}[\Lambda_2]$. This should be contrasted with our results for integer spin quantization of the 2D bosonic phase in Fig. 1. We obtain a Chern invariant of

$$C = m(0) - m(\infty) = \frac{1}{2} (\text{sgn}[\Lambda_0] + \text{sgn}[\Lambda_2]). \quad (58)$$

The phase is only nontrivial $C = \pm 1$ when $\Lambda_0 \Lambda_2 > 0$, necessitating a zero in the effective mass $\Lambda(k) = 0$ —precisely at $ka = \sqrt{\Lambda_0/\Lambda_2}$. This is the simplest realization of a fermionic Chern insulator [54]. Notice that in two dimensions, the Hall conductivity σ_H for the photon plays an analogous role as the Dirac mass Λ for the electron.

The electronic edge state has a similar interpretation as the photon, but for spin-1/2 particles. Imposing open boundary conditions, a unidirectional edge state is revealed, $\psi_{\pm}(x, y) = \psi_{\pm}(x) e^{ik_y y}$,

$$\psi_{\pm}(x) = \psi_0 \begin{bmatrix} 1 \\ \pm i \end{bmatrix} (e^{-\eta_1 x} - e^{-\eta_2 x}), \quad (59)$$

corresponding to a $C = \pm 1$ phase. The decay lengths have an identical form,

$$\eta_{1,2} = \frac{1}{2a^2 |\Lambda_2|} \left\{ v \pm \sqrt{v^2 + 4\Lambda_2 a^2 [\Lambda_2 (k_y a)^2 - \Lambda_0]} \right\}, \quad (60)$$

and the edge state is massless $E_{\pm} = \pm v k_y$, propagating in opposite directions depending on the phase. Furthermore, the edge state is spin-1/2 helically quantized, $\frac{1}{2} \hat{\mathbf{k}} \cdot \boldsymbol{\sigma} \psi_{\pm} = \frac{1}{2} \sigma_y \psi_{\pm} = \pm \frac{1}{2} \psi_{\pm}$, equating to a spin-up or spin-down electron for $C = 1$ or $C = -1$ respectively. The striking similarity of Maxwell bosons and Dirac fermions is shown in Fig. 7. A diagram of the electronic topological edge state is displayed in Fig. 7(b) and a plot of the probability density is given in Fig. 7(d).

VI. EXPERIMENTAL SEARCH AND CONCLUSIONS

The standard approach of characterizing TRS broken fermionic phases is dc transport measurements (charge and spin Hall conductivity) or Faraday rotation angles at THz frequencies. It should be noted that the former measurement gives information at zero frequency and zero momentum $\sigma_H(0, 0)$ whereas the latter experiment characterizes matter at finite frequency but close to zero momentum $\sigma_H(\omega, 0)$. Our predictions of photon spin quantization and bosonic phases are fundamentally tied to $\sigma_H(\omega, k)$. This is a formidable challenge and therefore, for completeness, we suggest two experimental approaches.

A. Momentum-resolved electron energy-loss spectroscopy of gyrotropic plasmas

The high-frequency $\omega > 0$ and subwavelength $k > 0$ properties of matter can be probed by momentum-resolved electron energy-loss spectroscopy (k EELS) [74]. Here, highly energetic electrons pass through matter and their energy loss, as well as their momentum loss, is measured to understand the bulk light-matter excitations. Fundamentally different from conventional STEM-EELS [75], this approach can also give insight into high momentum waves through scattering angle measurement of electrons passing through matter. We anticipate nonlocal gyrotropic plasmas to be ideal candidates for topological bosonic phases of matter and probing with k EELS.

B. Cold atom near-field probes of nonlocal optical conductivity

Dynamical (high-frequency) conductivity is regularly studied by conventional tools such as ellipsometry and Faraday rotation using incident optical beams. However, the momentum carried by light waves is negligible compared to the Fermi momentum of electrons. Therefore, the large momentum $k > 0$ behavior of the conductivity requires fundamentally different probes. One approach is to use spontaneous emission from cold atoms in the near field to investigate deep subwavelength response parameters of our predicted bosonic phases of matter. This is feasible since the GHz splitting in Rydberg atoms [76] and low-frequency gyrotropic response in systems such as quantum wells are comparable [32]. Recent work has shown trapping of cold atoms near photonic nanostructures [77]—a promising route for probing topological properties of matter.

C. Conclusions

In summary, we have developed the complete continuum field theory describing all 2+1D topological bosonic phases of the photon; incorporating both temporal and spatial dispersion as a necessary generalization. The topological phases are intimately connected to photon spin-1 quantization, with non-locality being imperative to properly characterize the high- k global behavior. Two unique bosonic phases are predicted: an even parity phase $C = \pm 2$ which is understood in interacting bosonic systems, and an odd parity phase $C = \pm 1$ which has no immediate interpretation but presents possibly unexplored physics. We have studied the even parity phase $C = \pm 2$ utilizing a nonlocal Hall conductivity and reveal a single topologically protected unidirectional photon at the

edge. This photon is helically quantized (spin-1), immune to backscattering, defects, and exists at the boundary of the $C = \pm 2$ bosonic phase and any interface—even vacuum. To validate our theory, we have compared all the low-energy Maxwell phenomena to its supersymmetric Dirac counterpart, confirming that even parity bosonic phases $C = \pm 2$ are the exact analog of traditional fermionic phases $C = \pm 1$.

ACKNOWLEDGMENTS

This research was supported by the Defense Advanced Research Projects Agency (Grant No. N66001-17-1-4048) and the National Science Foundation (Grant No. EFMA-1641101). We also thank Dr. C. Cortes for insightful discussions.

APPENDIX A: 2+1D ELECTROMAGNETIC LAGRANGIAN

To understand the two-dimensional behavior of photons [41], we start with the electromagnetic Lagrangian coupled to a conserved current $\partial_\mu J^\mu = 0$,

$$\mathcal{L} = -\frac{1}{4}F^{\mu\nu}F_{\mu\nu} - A_\mu J^\mu, \quad F^{\mu\nu} = \partial^\mu A^\nu - \partial^\nu A^\mu, \quad (A1)$$

which is exact in any space-time dimension. The conservation of charge ensures the action $S = \int d^d x dt \mathcal{L}$ is gauge invariant, where d is the spatial dimension. For $d = 2$, the motion of charge is restricted to the x - y plane,

$$J^\mu = (\rho, J_x, J_y), \quad \dot{\rho} + \partial_i J^i = 0. \quad (A2)$$

Similarly, planar currents restrict the spatial degrees of freedom of the gauge potential A^μ ,

$$A^\mu = (\phi, A_x, A_y). \quad (A3)$$

This implies there are only two components of the electric field and one for the magnetic field,

$$E_i = -\partial_i \phi - \dot{A}_i, \quad B_z = \epsilon^{ij} \partial_i A_j = \partial_x A_y - \partial_y A_x, \quad (A4)$$

such that exclusively transverse-magnetic (TM) waves propagate within a 2D material. This makes physical sense since the circulation of currents can only generate magnetic fields in a single \hat{z} direction. Note that $\epsilon_{ij} = -\epsilon_{ji}$ is the 2D antisymmetric matrix and should not be confused with the permittivity.

Varying the action with respect to A^μ , we arrive at the familiar equations of motion,

$$\partial_\mu F^{\mu\nu} = J^\nu, \quad \tilde{F}^\mu = \frac{1}{2}\epsilon^{\mu\nu\rho} F_{\nu\rho}, \quad \partial_\mu \tilde{F}^\mu = 0. \quad (A5)$$

Notice the dual equation \tilde{F}_μ is slightly different in two dimensions, which arises from the fact there are only three unique components of the electromagnetic field. We can express the equations of motion directly in terms of E_i and B_z ,

$$\partial_i E^i = \rho, \quad \epsilon_{ij} \partial^j B_z - \dot{E}_i = J_i, \quad \dot{B}_z + \epsilon^{ij} \partial_i E_j = 0. \quad (A6)$$

These are precisely Maxwell's equations in two dimensions.

We are most interested in the response of a bulk 2D material so it is convenient to represent the induced charges in terms of the polarization P_i and magnetization M_z densities,

$$\rho = -\partial_i P^i, \quad J_i = \dot{P}_i + \epsilon_{ij} \partial^j M_z. \quad (A7)$$

Substituting into the equations of motion, we define the electric D_i and magnetic B_z displacement fields as

$$\dot{D}_i - \epsilon_{ij} \partial^j H_z = 0, \quad \dot{B}_z + \epsilon^{ij} \partial_i E_j = 0, \quad (\text{A8})$$

which is simply the linear superposition of

$$D_i = E_i + P_i, \quad B_z = H_z + M_z. \quad (\text{A9})$$

The wave equation in Eq. (2) follows immediately after substituting for the linear-response function \mathcal{M} and defining the column vector $f = [E_x \ E_y \ H_z]^\top$ for the TM state.

APPENDIX B: ELECTROMAGNETIC HAMILTONIAN AND POLARITON EIGENSTATES

Here, we show that the response function \mathcal{M} is derived from a first-order in time Hamiltonian. Utilizing the decomposition in Eq. (6), we expand in terms of three-component oscillator variables ψ_α by defining

$$\psi_\alpha = \frac{C_{\alpha\mathbf{k}} f}{\omega - \omega_{\alpha\mathbf{k}}}, \quad \omega \psi_\alpha = \omega_{\alpha\mathbf{k}} \psi_\alpha + C_{\alpha\mathbf{k}} f, \quad (\text{B1})$$

which is first order in time. Similarly, we back-substitute Eq. (6) into Eq. (2) to obtain

$$\omega f = \left[\mathcal{H}_0(\mathbf{k}) + \sum_\alpha \omega_{\alpha\mathbf{k}}^{-1} C_{\alpha\mathbf{k}}^\dagger C_{\alpha\mathbf{k}} \right] f + \sum_\alpha C_{\alpha\mathbf{k}}^\dagger \psi_\alpha. \quad (\text{B2})$$

The first term represents the vacuum equations and self-energy of the electromagnetic field, while the second is the linear coupling to the oscillators. By combining Eq. (B1) and (B2) into a single algebraic matrix, the complete electromagnetic Hamiltonian emerges,

$$H(\mathbf{k}) = \begin{bmatrix} \mathcal{H}_0(\mathbf{k}) + \sum_\alpha \omega_{\alpha\mathbf{k}}^{-1} C_{\alpha\mathbf{k}}^\dagger C_{\alpha\mathbf{k}} & C_{1\mathbf{k}}^\dagger & C_{2\mathbf{k}}^\dagger & \cdots \\ C_{1\mathbf{k}} & \omega_{1\mathbf{k}} & 0 & \cdots \\ C_{2\mathbf{k}} & 0 & \omega_{2\mathbf{k}} & \cdots \\ \vdots & \vdots & \vdots & \ddots \end{bmatrix}. \quad (\text{B3})$$

The Hermitian equation $Hu = \omega u$ characterizes the dynamics of the entire electromagnetic problem in a 2D material. u constitutes the cumulative state vector of the photon + all oscillator degrees of freedom,

$$u = [f \ \psi_1 \ \psi_2 \ \dots]^\top. \quad (\text{B4})$$

Notice that contraction of u naturally reproduces the energy density upon summation over all degrees of freedom,

$$u^\dagger u = f^\dagger f + f^\dagger \sum_\alpha \frac{C_{\alpha\mathbf{k}}^\dagger C_{\alpha\mathbf{k}}}{(\omega - \omega_{\alpha\mathbf{k}})^2} f = f^\dagger \bar{\mathcal{M}} f, \quad (\text{B5})$$

with $\bar{\mathcal{M}} = \partial_\omega(\omega \mathcal{M}) > 0$ always positive definite.

Eigenstates of the Hamiltonian are collective excitations of oscillators coupled to the electromagnetic field,

$$H_{\mathbf{k}} u_{n\mathbf{k}} = \omega_{n\mathbf{k}} u_{n\mathbf{k}}, \quad (\text{B6})$$

and are manifestly bosonic quasiparticles. These are the n nontrivial roots of the characteristic equation,

$$\det[\mathcal{H}_0(\mathbf{k}) - \omega \mathcal{M}(\omega, \mathbf{k})] = 0, \quad \omega = \omega_n(\mathbf{k}), \quad (\text{B7})$$

which generates the eigenenergies at any particular momenta. Normalization of each mode is given concisely as $1 = f_{n\mathbf{k}}^\dagger \bar{\mathcal{M}}(\omega_{n\mathbf{k}}, \mathbf{k}) f_{n\mathbf{k}}$.

APPENDIX C: CONTINUUM REGULARIZATION

To adequately describe a continuum topological field theory, the Hamiltonian must approach a directionally independent value in the asymptotic limit $\lim_{k \rightarrow \infty} H(\mathbf{k}) \rightarrow H(k)$, such that the system is connected at infinity [52]. This is the continuum equivalent of a periodic boundary condition since all limits at $k \rightarrow \infty$ are mapped into a single point (i.e., one-point compactification). We can prove the Chern number is quantized by analyzing the Berry phase over all momentum. Continuum regularization necessitates the following condition:

$$\oint_\infty \mathbf{A}_n \cdot d\mathbf{k} = -2\pi \sum_i p_i + \iint_{\mathbb{R}^2} F_n d^2\mathbf{k} = 2\pi p, \quad (\text{C1})$$

with p and $p_i \in \mathbb{Z}$ an integer. Here, $\mathbf{A}_n(\mathbf{k}) = -i u_{n\mathbf{k}}^\dagger \partial_{\mathbf{k}} u_{n\mathbf{k}}$ is the Berry connection of any particular eigenstate and $F_n(\mathbf{k}) = \hat{\mathbf{z}} \cdot [\partial_{\mathbf{k}} \times \mathbf{A}_n(\mathbf{k})]$ is the Berry curvature. The path integral is performed over a closed loop at infinity $k = \infty$, which is equivalent to the Berry flux over all momentum space \mathbb{R}^2 minus any singular points in the connection. p_i label these singular points of the Berry connection $\mathbf{A}_n(\mathbf{k}_i)$ which contribute an integer unit of Berry flux at a particular momentum \mathbf{k}_i . The Chern number $C_n \in \mathbb{Z}$ is the summation over all such singularities,

$$C_n = p + \sum_i p_i = \frac{1}{2\pi} \iint_{\mathbb{R}^2} F_n d^2\mathbf{k}. \quad (\text{C2})$$

For Eq. (C2) to hold, we see that the eigenstates must approach a directionally independent value in the asymptotic limit, up to a possible U(1) gauge,

$$\lim_{k \rightarrow \infty} u_n(\mathbf{k}) \rightarrow u_n(k) \exp[i \chi_n(\mathbf{k})]. \quad (\text{C3})$$

When this is the case, the closed loop at infinity $k = \infty$ is determined purely by the gauge,

$$\oint_\infty \mathbf{A}_n \cdot d\mathbf{k} = \oint_\infty \partial_{\mathbf{k}} \chi_n \cdot d\mathbf{k} = \chi_n|_0^{2\pi} = 2\pi p, \quad (\text{C4})$$

which is guaranteed to be an integer multiple of 2π . Hence, Chern numbers are quantized.

For completeness, we note that the Berry connection can be simplified slightly to

$$\mathbf{A}_n(\mathbf{k}) = -i f_{n\mathbf{k}}^\dagger \bar{\mathcal{M}}(\omega_{n\mathbf{k}}, \mathbf{k}) \partial_{\mathbf{k}} f_{n\mathbf{k}} + f_{n\mathbf{k}}^\dagger \mathcal{A}(\omega_{n\mathbf{k}}, \mathbf{k}) f_{n\mathbf{k}}, \quad (\text{C5})$$

where \mathcal{A} is the Berry connection arising from the oscillators,

$$\mathcal{A}(\omega, \mathbf{k}) = -i \sum_\alpha \frac{C_{\alpha\mathbf{k}}^\dagger \partial_{\mathbf{k}} C_{\alpha\mathbf{k}}}{(\omega - \omega_{\alpha\mathbf{k}})^2}. \quad (\text{C6})$$

- [1] K. V. Klitzing, G. Dorda, and M. Pepper, New Method for High-Accuracy Determination of the Fine-Structure Constant Based on Quantized Hall Resistance, *Phys. Rev. Lett.* **45**, 494 (1980).
- [2] R. B. Laughlin, Quantized Hall conductivity in two dimensions, *Phys. Rev. B* **23**, 5632 (1981).
- [3] D. J. Thouless, M. Kohmoto, M. P. Nightingale, and M. den Nijs, Quantized Hall Conductance in a Two-Dimensional Periodic Potential, *Phys. Rev. Lett.* **49**, 405 (1982).
- [4] Y. Ikebe, T. Morimoto, R. Masutomi, T. Okamoto, H. Aoki, and R. Shimano, Optical Hall Effect in the Integer Quantum Hall Regime, *Phys. Rev. Lett.* **104**, 256802 (2010).
- [5] C. L. Kane and E. J. Mele, Quantum Spin Hall Effect in Graphene, *Phys. Rev. Lett.* **95**, 226801 (2005).
- [6] B. A. Bernevig, T. L. Hughes, and S.-C. Zhang, Quantum spin hall effect and topological phase transition in hgte quantum wells, *Science* **314**, 1757 (2006).
- [7] T. Lan, L. Kong, and X.-G. Wen, Theory of (2+1)-dimensional fermionic topological orders and fermionic/bosonic topological orders with symmetries, *Phys. Rev. B* **94**, 155113 (2016).
- [8] X. Chen, Z.-C. Gu, Z.-X. Liu, and X.-G. Wen, Symmetry-protected topological orders in interacting bosonic systems, *Science* **338**, 1604 (2012).
- [9] A. Vishwanath and T. Senthil, Physics of Three-Dimensional Bosonic Topological Insulators: Surface-Deconfined Criticality and Quantized Magnetoelectric Effect, *Phys. Rev. X* **3**, 011016 (2013).
- [10] M. A. Metlitski, C. L. Kane, and M. P. A. Fisher, Bosonic topological insulator in three dimensions and the statistical witten effect, *Phys. Rev. B* **88**, 035131 (2013).
- [11] T. Senthil and M. Levin, Integer Quantum Hall Effect for Bosons, *Phys. Rev. Lett.* **110**, 046801 (2013).
- [12] Y.-M. Lu and A. Vishwanath, Theory and classification of interacting integer topological phases in two dimensions: A chern-simons approach, *Phys. Rev. B* **86**, 125119 (2012).
- [13] X. Chen, Z.-X. Liu, and X.-G. Wen, Two-dimensional symmetry-protected topological orders and their protected gapless edge excitations, *Phys. Rev. B* **84**, 235141 (2011).
- [14] T. Van Mechelen and Z. Jacob, Dirac-Maxwell correspondence: Spin-1 bosonic topological insulator, [arXiv:1708.08192](https://arxiv.org/abs/1708.08192).
- [15] M. Hafezi, S. Mittal, J. Fan, A. Migdall, and J. M. Taylor, Imaging topological edge states in silicon photonics, *Nat. Photon.* **7**, 1001 (2013).
- [16] T. Karzig, C.-E. Bardyn, N. H. Lindner, and G. Refael, Topological Polaritons, *Phys. Rev. X* **5**, 031001 (2015).
- [17] Y. Hadad, V. Vitelli, and A. Alu, Solitons and propagating domain walls in topological resonator arrays, *ACS Photon.* **4**, 1974 (2017).
- [18] G. De Nitti and M. Lein, Symmetry Classification of Topological Photonic Crystals, [arXiv:1710.08104](https://arxiv.org/abs/1710.08104).
- [19] Z.-C. Gu, Z. Wang, and X.-G. Wen, Classification of two-dimensional fermionic and bosonic topological orders, *Phys. Rev. B* **91**, 125149 (2015).
- [20] L. Lu, L. Fu, J. D. Joannopoulos, and M. Soljacic, Weyl points and line nodes in gyroid photonic crystals, *Nat. Photon.* **7**, 294 (2013).
- [21] Z. Wang, Y. Chong, J. D. Joannopoulos, and M. Soljacic, Observation of unidirectional backscattering-immune topological electromagnetic states, *Nature (London)* **461**, 772 (2009).
- [22] Z. Wang and S. Fan, Optical circulators in two-dimensional magneto-optical photonic crystals, *Opt. Lett.* **30**, 1989 (2005).
- [23] M. C. Rechtsman, J. M. Zeuner, Y. Plotnik, Y. Lumer, D. Podolsky, F. Dreisow, S. Nolte, M. Segev, and A. Szameit, Photonic floquet topological insulators, *Nature (London)* **496**, 196 (2013), letter .
- [24] A. B. Khanikaev, S. Hossein Mousavi, W.-K. Tse, M. Kargarian, A. H. MacDonald, and G. Shvets, Photonic topological insulators, *Nat. Mater.* **12**, 233 (2013).
- [25] A. Slobozhanyuk, S. H. Mousavi, X. Ni, D. Smirnova, Y. S. Kivshar, and A. B. Khanikaev, Three-dimensional all-dielectric photonic topological insulator, *Nat. Photon.* **11**, 130 (2017), article .
- [26] C. He, X.-C. Sun, X.-P. Liu, M.-H. Lu, Y. Chen, L. Feng, and Y.-F. Chen, Photonic topological insulator with broken time-reversal symmetry, *Proc. Natl. Acad. Sci. USA* **113**, 4924 (2016).
- [27] S. Raghu and F. D. M. Haldane, Analogs of quantum-hall-effect edge states in photonic crystals, *Phys. Rev. A* **78**, 033834 (2008).
- [28] J. Koch, A. A. Houck, K. Le Hur, and S. M. Girvin, Time-reversal-symmetry breaking in circuit-QED-based photon lattices, *Phys. Rev. A* **82**, 043811 (2010).
- [29] D. Jaksch and P. Zoller, Creation of effective magnetic fields in optical lattices: the hofstadter butterfly for cold neutral atoms, *New J. Phys.* **5**, 56 (2003).
- [30] M. G. Silveirinha, Chern invariants for continuous media, *Phys. Rev. B* **92**, 125153 (2015).
- [31] M. G. Silveirinha, $\mathcal{P} \cdot \mathcal{T} \cdot \mathcal{D}$ symmetry-protected scattering anomaly in optics, *Phys. Rev. B* **95**, 035153 (2017).
- [32] D. Jin, L. Lu, Z. Wang, C. Fang, J. D. Joannopoulos, M. Soljacic, L. Fu, and N. X. Fang, Topological magnetoplasmon, *Nat. Commun.* **7**, 13486 (2016).
- [33] L.-K. Shi and J. C. W. Song, Plasmon Geometric Phase and Plasmon Hall Shift, *Phys. Rev. X* **8**, 021020 (2018).
- [34] I. Bialynicki-Birula and Z. Bialynicka-Birula, Berry's phase in the relativistic theory of spinning particles, *Phys. Rev. D* **35**, 2383 (1987).
- [35] M. Stone, Berry phase and anomalous velocity of weyl fermions and maxwell photons, *Int. J. Mod. Phys. B* **30**, 1550249 (2016).
- [36] M. Z. Hasan and C. L. Kane, Colloquium: Topological insulators, *Rev. Mod. Phys.* **82**, 3045 (2010).
- [37] S. M. Barnett, L. Allen, R. P. Cameron, C. R. Gilson, M. J. Padgett, F. C. Speirits, and A. M. Yao, On the natures of the spin and orbital parts of optical angular momentum, *J. Opt. (Bristol, UK)* **18**, 064004 (2016).
- [38] K. Y. Bliokh and F. Nori, Transverse and longitudinal angular momenta of light, *Phys. Rep.* **592**, 1 (2015).
- [39] T. V. Mechelen and Z. Jacob, Universal spin-momentum locking of evanescent waves, *Optica* **3**, 118 (2016).
- [40] F. Kalhor, T. Thundat, and Z. Jacob, Universal spin-momentum locked optical forces, *Appl. Phys. Lett.* **108**, 061102 (2016).
- [41] G. V. Dunne, Aspects of chern-simons theory, in *Aspects Topologiques de la Physique en Basse Dimension. Topological Aspects of Low Dimensional Systems*, edited by A. Comtet, T. Jolicœur, S. Ouvry, and F. David (Springer, Berlin, 1999), p. 177.
- [42] D. Boyanovsky, R. Blankenbecler, and R. Yahalom, Physical origin of topological mass in 2+1 dimensions, *Nucl. Phys. B* **270**, 483 (1986).
- [43] K. Ziegler, Delocalization of 2d Dirac Fermions: The Role of a Broken Supersymmetry, *Phys. Rev. Lett.* **80**, 3113 (1998).

- [44] S. J. Gates Jr, M. T. Grisaru, M. Rocek, and W. Siegel, Superspace, or One thousand and one lessons in supersymmetry, *Front. Phys.* **58**, 1 (1983).
- [45] L. D. Landau, J. S. Bell, M. J. Kearsley, L. P. Pitaevskii, E. M. Lifshitz, and J. B. Sykes, *Electrodynamics of Continuous Media* (Elsevier, New York, 2013), Vol. 8.
- [46] S. A. R. Horsley and T. G. Philbin, Canonical quantization of electromagnetism in spatially dispersive media, *New J. Phys.* **16**, 013030 (2014).
- [47] S. T. Ivanov and N. I. Nikolaev, Singular waves along the boundary of gyrotropic plasma, *J. Phys. D: Appl. Phys.* **29**, 1107 (1996).
- [48] A. Eroglu, *Wave Propagation and Radiation in Gyrotropic and Anisotropic Media* (Springer Science & Business Media, New York, 2010).
- [49] W.-Y. Shan, H.-Z. Lu, and S.-Q. Shen, Effective continuous model for surface states and thin films of three-dimensional topological insulators, *New J. Phys.* **12**, 043048 (2010).
- [50] A. Medhi and V. B. Shenoy, Continuum theory of edge states of topological insulators: variational principle and boundary conditions, *J. Phys.: Condens. Matter* **24**, 355001 (2012).
- [51] S.-Q. Shen, W.-Y. Shan, and H.-Z. Lu, Topological insulator and the dirac equation, *SPIN* **01**, 33 (2011).
- [52] S. Ryu, A. P. Schnyder, A. Furusaki, and A. W. W. Ludwig, Topological insulators and superconductors: tenfold way and dimensional hierarchy, *New J. Phys.* **12**, 065010 (2010).
- [53] J. R. Munkres, *Topology*, Featured Titles for Topology Series (Prentice-Hall, Englewood Cliffs, NJ, 2000).
- [54] B. A. Bernevig and T. L. Hughes, *Topological Insulators and Topological Superconductors* (Princeton University Press, Princeton, NJ, 2013).
- [55] V. M. Agranovich and V. Ginzburg, *Crystal Optics with Spatial Dispersion, and Excitons* (Springer Science & Business Media, New York, 2013), Vol. 42.
- [56] A. A. Rukhadze and V. P. Silin, Electrodynamics of media with spatial dispersion, *Sov. Phys. Usp.* **4**, 459 (1961).
- [57] D. Hestenes, Point groups and space groups in geometric algebra, in *Applications of Geometric Algebra in Computer Science and Engineering*, edited by L. Dorst, C. Doran, and J. Lasenby (Birkhäuser Boston, Boston, 2002), p. 3.
- [58] J. F. Nye, *Physical Properties of Crystals: Their Representation by Tensors and Matrices* (Oxford University Press, New York, 1985).
- [59] B. C. Hall, *Lie Groups, Lie Algebras, and Representations*, Graduate Texts in Mathematics Vol. 222 (Springer International Publishing, Cham, 2015).
- [60] C. Fang, M. J. Gilbert, and B. A. Bernevig, Bulk topological invariants in noninteracting point group symmetric insulators, *Phys. Rev. B* **86**, 115112 (2012).
- [61] N. R. Heckenberg, R. McDuff, C. P. Smith, H. Rubinsztein-Dunlop, and M. J. Wegener, Laser beams with phase singularities, *Opt. Quantum Electron.* **24**, S951 (1992).
- [62] T.-S. Zeng, W. Zhu, and D. N. Sheng, Bosonic integer quantum hall states in topological bands with chern number two, *Phys. Rev. B* **93**, 195121 (2016).
- [63] N. Read, Lowest-landau-level theory of the quantum hall effect: The fermi-liquid-like state of bosons at filling factor one, *Phys. Rev. B* **58**, 16262 (1998).
- [64] Y. Zheng and T. Ando, Hall conductivity of a two-dimensional graphite system, *Phys. Rev. B* **65**, 245420 (2002).
- [65] G. Jotzu, M. Messer, R. Desbuquois, M. Lebrat, T. Uehlinger, D. Greif, and T. Esslinger, Experimental realization of the topological haldane model with ultracold fermions, *Nature (London)* **515**, 237 (2014).
- [66] O. Takayama, L.-C. Crasovan, S. K. Johansen, D. Mihalache, D. Artigas, and L. Torner, Dyakonov surface waves: A review, *Electromagnetics* **28**, 126 (2008).
- [67] P. Halevi and R. Fuchs, Generalised additional boundary condition for non-local dielectrics. i. reflectivity, *J. Phys. C* **17**, 3869 (1984).
- [68] I. M. Gelfand, S. V. Fomin, and R. A. Silverman, *Calculus of Variations*, Dover Books on Mathematics (Dover, New York, 2000).
- [69] Y. Hatsugai, Chern Number and Edge States in the Integer Quantum Hall Effect, *Phys. Rev. Lett.* **71**, 3697 (1993).
- [70] J. C. Avila, H. Schulz-Baldes, and C. Villegas-Blas, Topological invariants of edge states for periodic two-dimensional models, *Math. Phys., Anal. Geom.* **16**, 137 (2013).
- [71] N. Nagaosa, J. Sinova, S. Onoda, A. H. MacDonald, and N. P. Ong, Anomalous Hall effect, *Rev. Mod. Phys.* **82**, 1539 (2010).
- [72] F. D. M. Haldane, Model for a Quantum Hall Effect without Landau Levels: Condensed-Matter Realization of the “Parity Anomaly”, *Phys. Rev. Lett.* **61**, 2015 (1988).
- [73] E. Fradkin, E. Dagotto, and D. Boyanovsky, Physical Realization of the Parity Anomaly in Condensed Matter Physics, *Phys. Rev. Lett.* **57**, 2967 (1986).
- [74] P. Shekhar, M. Malac, V. Gaiand, N. Dalili, A. Meldrum, and Z. Jacob, Momentum-resolved electron energy loss spectroscopy for mapping the photonic density of states, *ACS Photon.* **4**, 1009 (2017).
- [75] J. A. Scholl, A. L. Koh, and J. A. Dionne, Quantum plasmon resonances of individual metallic nanoparticles, *Nature (London)* **483**, 421 (2012).
- [76] M. Saffman, T. G. Walker, and K. Mølmer, Quantum information with rydberg atoms, *Rev. Mod. Phys.* **82**, 2313 (2010).
- [77] A. Goban, C.-L. Hung, J. D. Hood, S.-P. Yu, J. A. Muniz, O. Painter, and H. J. Kimble, Superradiance for Atoms Trapped Along a Photonic Crystal Waveguide, *Phys. Rev. Lett.* **115**, 063601 (2015).